Available online at www.sciencedirect.com
ScienceDirect
Remote Sensing of Environment 104 (2006) 361–373
Remote Sensing of Environment
www.elsevier.com/locate/rse

A ground-based radar backscatter investigation in the percolation zone of the Greenland ice sheet

Julian B.T. Scott [a], Doug Mair [b,*], Pete Nienow [a], Victoria Parry [a], Elizabeth Morris [c]

[a] University of Edinburgh, Edinburgh, United Kingdom
[b] University of Aberdeen, Aberdeen, United Kingdom
[c] The British Antarctic Survey, Cambridge, United Kingdom

Received 22 December 2005; received in revised form 5 April 2006; accepted 17 May 2006

Abstract

Satellite radar altimeters and scatterometers deployed over ice sheets experience backscatter from the surface and from within the snowpack, termed surface and volume backscatter respectively. In order to assess the errors in satellite altimeter measurements it is vital to know where the return is originating from in the snowpack. This return can vary spatially and temporally. Seasonal variations in the volume backscatter can be a major complicating factor in the radar return from the percolation zone. Ground-based step-frequency radar was deployed in the percolation zone of the Greenland Ice Sheet at ~1945 m elevation (69 51N, 47 15W). Previous measurements in this area made by scientists from the Byrd Polar Research Centre and the University of Kansas, undertaken prior to summer melt events, have shown the strongest backscatter from ice features at around 1 m depth buried beneath the previous end-of-summer surface. In autumn 2004, radar measurements in the Ku band with bandwidths of 1 and 8 GHz were made alongside detailed stratigraphic observations within a 1 km^2 site. The radar results revealed no continuous reflecting horizons in the upper 3.5 m of the firn. Shallow cores and snowpits also indicated that there were no spatially continuous stratigraphic horizons across the study site. An average electromagnetic wave velocity of $2.11 \pm 0.05 \times 10^8$ m s^{-1} was determined for the upper metre of the firn. Surface and volume backscatter at vertical incidence were calculated using a standard model. The contribution of the surface backscatter to the total backscatter was on average 6 dB higher than that of the volume backscatter. However, at the higher 8 GHz bandwidth the strongest return frequently originated not from the surface but from within the upper 30 cm of the snowpack, most probably from thin ice layers. At 1 GHz bandwidth these ice layers were not always resolved; their return merged with the surface return, causing it to broaden, with the peak and leading edge moving down. Modelling using density and thickness measurements from shallow cores and snowpits showed that the backscatter from these shallow, thin ice layers could be stronger than the surface return owing to constructive interference from the top and base of the layers.
© 2006 Elsevier Inc. All rights reserved.

Keywords: Radar backscatter; Greenland; Ice sheet

1. Introduction

Calculation of changes in the surface elevation of ice masses including the Greenland and Antarctic ice sheets is important for assessing the impacts of climate change on glacier mass balance. To date the best way of obtaining large-scale elevation estimates for these areas is by satellite (Bindschadler, 1998). However, elevation measurements by satellite radar altimeters are affected by topography, particularly on the scale of the radar footprint (1–10 km), and by the volume return from within the snowpack (Legresy & Remy, 1997; Wingham, 1995). Accurate measurements of elevation change from radar satellites are more difficult to obtain around the edges of these ice sheets than in the centres. This is largely because of the greater surface gradients near ice sheet margins but the difficulty will be compounded if temporal variations in the radar backscatter result from complex seasonal density variations in surface snow/firn layers in the percolation and wet snow zones (Benson, 1962). Seasonal variations in the volume backscatter from within the snowpack may be particularly significant in these zones. During the summer melt season ice lenses and other features may form in the snowpack as a consequence of surface melt, percolation to depth within the snowpack and refreezing thereby significantly changing snowpack density profiles. It is therefore important to examine whether these density changes cause variations in volume backscatter that may

* Corresponding author. Tel.: +44 1224 272326.
E-mail address: d.mair@abdn.ac.uk (D. Mair).

0034-4257/$ - see front matter © 2006 Elsevier Inc. All rights reserved.
doi:10.1016/j.rse.2006.05.009

to −25 °C but the keyboard and monitor ceased to function properly at around −30 °C. Frequency domain data was converted to a synthesised time domain return by using a Fourier transform in Matlab with a hamming window to control side lobes. Static radar measurements were made from 2 to 18 GHz, which at a step size of 909 kHz needed 17,601 frequency points. To recreate the desired bandwidth, a subset of these points was taken around the required centre frequency and transformed separately. The centre frequency used for the experiments presented in this paper is in the Ku band to ensure relevance to satellite radar data collected over Greenland such as ERS 1 and 2, NSCAT and QSCAT (Drinkwater et al., 2001).

2.2. Calibration of the radar

The radar was initially calibrated using a trihedral corner reflector. This has a maximum backscattering cross section, σ_{max}, along its axis of symmetry, given by (Ulaby et al., 1982, p. 776):

$$\sigma_{max} = \frac{4\pi}{\lambda^2} A_{eff}^2 \tag{1}$$

$$A_{eff} = \frac{l^2}{\sqrt{12}} \tag{2}$$

where λ is the wavelength of the radiation, A_{eff} is the effective area and l is the length of the sides, in this case 25 cm. It can be assumed that with sufficient distance from the antennas the corner reflector behaves as a point target, therefore the power return, P_r, is given by the radar equation (Ulaby & Dobson, 1989):

$$P_r = \frac{P_t G_0^2 \lambda^2}{(4\pi)^3 R^4} \sigma \tag{3}$$

where P_t is the transmitted power, G_0 is the maximum gain of the radar along its axis of symmetry, and R is the distance for the antennas' phase centre. In order to calibrate the radar, the corner reflector was positioned two metres above the ground, supported by a cardboard tube to prevent any high magnitude additional reflections. Measurements were taken with the antennas pointing directly at the corner reflector at increasing distances along its axis of symmetry. A plot of P_t/P_r against R^4 (Fig. 2) allows calculation of G_0 from the gradient (Eq. (3)) because σ is known from Eqs. (1) and (2). The closest point to the radar does not follow the trend because the corner reflector is no longer acting as a point target and is within the edge of the Fresnel region (outer part of near field) which extends to 1.2 m for the antennas used. This point can therefore be ignored in the calculation. Using a bandwidth of 1 GHz and at a centre frequency of 13.5 GHz, $G_0 = 0.0464$. For the measurements described in this paper the snow surface was in the far field for static measurements but in the near field while profiling over 1.5 km (pulled on sledge by skidoo).

2.3. Backscatter power with depth from a distributed target

For accurate calculation of backscatter power from a distributed target, like a snowpack, the antenna pattern and illuminated area need to be known. Assuming backscatter does not vary significantly with angle for the system employed at vertical incidence the return power is given by the following equation (Ulaby & Dobson, 1989):

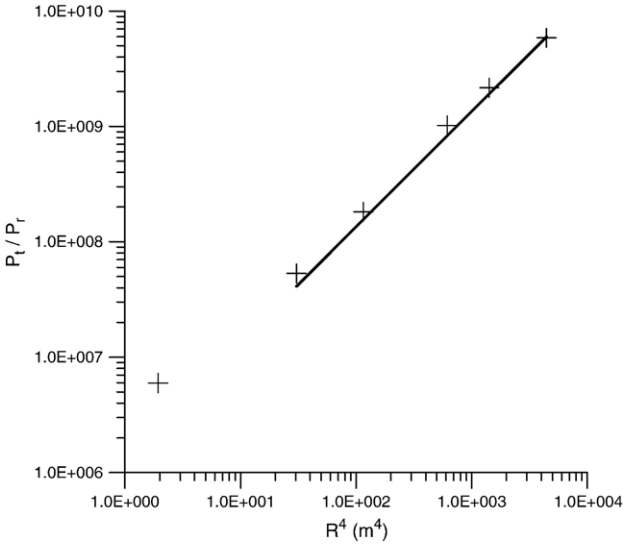

Fig. 2. Power calibration graph.

$$P_r = \frac{P_t \lambda^2 G_0^2}{(4\pi)^3} . \sigma^0 \int_A \int \frac{g^2(\theta,\phi)}{R^4} dA \tag{4}$$

where the backscattering coefficient, σ^0, replaces the backscattering cross section and A is the area illuminated by the radar beam. The limitations on assuming σ^0 is constant are described in detail by Ulaby et al. (1982, p. 755). At vertical incidence σ^0 can fall off rapidly with angle; this may mean σ^0 will be under-estimated with this system but, without extensive measurements of backscatter with angle it is difficult to account for this. The results of Jezek et al. (1994) show that, in the Ku band (13.3 GHz), the surface backscatter does not fall off rapidly with incident angle in the range 0–15°. This may, therefore, not be a significant problem. Nevertheless, we intend to measure backscatter as a function of incident angle during future work on Greenland.

The gain of the antennas, G, is now expressed as a combination of the maximum antenna gain and the angular gain pattern, $g(\theta,\phi)$ as follows:

$$G = G_0 g(\theta,\phi) \tag{5}$$

The system used here is effectively a beam-limited system (Ulaby et al., 1982) for all frequencies at bandwidths up to 3 GHz. It is also beam-limited at frequencies above 7 GHz for bandwidths up to 10 GHz. Assuming a flat surface and that the antenna gain pattern is equal in the θ and ϕ directions for these antennas, the area of illumination integral (Eq. (4)) is evaluated over the angle from the antenna axis using the substitution:

$$dA = 2\pi R^2 \sin\theta d\theta \tag{6}$$

where R is the distance from the antennas phase centre and is related to h, the height of the antennas above the ground by:

$$h = R\cos\theta \tag{7}$$

However, we are interested in not only the surface backscatter, but also the distribution of backscatter with depth. Using the wavefront of a conic beam the effective area illuminated can be calculated using the solid angle, Ω:

$$A = \Omega R^2 \tag{8}$$

$$\Omega = 2\pi(1-\cos\theta) \tag{9}$$

The distribution of the backscatter with depth, z, will be given by substituting the parameter $s(z)$ for the backscatter coefficient, σ^0, in Eq. (4) and calculating the illuminated area, which also varies with depth, using Eqs. (7) and (8). The parameter, $s(z)$, is similar to that used by Arthern et al. (2001), but is not always distinguished from σ in other papers (Zabel et al., 1995). It should be noted that z is only an apparent depth as returns can originate from off-nadir. Additionally, because there are multiple reflections within the firn, $s(z)$ should strictly be $s(t)=s(z/v_{\text{firn}})$ where, v_{firn}, is the velocity of electromagnetic radiation in the firn and, t, is time.

In this paper, we are interested in determining and examining variations in the backscatter response in conjunction with snow pit and ice core measurements of snow and firn density to a depth of several metres. In particular, we aim to determine the depths from which the main power returns are originating and whether this has any bearing on the calculation of the surface elevation from satellite radar altimeter measurements.

3. Field area

3.1. Location

Ground measurements were made from a base camp located at ~1945 m elevation (69 51N, 47 15W) in the middle of the percolation zone of the Greenland Ice Sheet. Detailed data on past climate and mass balance fluctuations are available at this location (hereafter referred to as T05) from measurements along the Expédition Glaciologique Internationale au Groenland (EGIG) line in 1990 and 1992 (Fischer et al., 1995). Measurements of the density and stratigraphy of near surface firn and snowpack properties were made within a 1 km^2 nested grid as shown in Fig. 1. These were made both in spring (April to May 2004) and autumn (August to September 2004), that is prior to and post summer melting. As part of the autumn campaign the step-frequency radar was also deployed. Radar measurements were made prior to the digging of snowpits and the taking of cores thus detailed near surface glaciological information was obtained at the same points as the radar returns. The size of the grid was chosen because radar volume backscatter over the km scale is the most relevant for comparison with satellite altimeters (Wingham, 1995) and 1 km^2 is the intended footprint of Cryosat. As a related part of the satellite calibration and validation activities during spring and autumn of 2004, measurement sites along the EGIG line were over flown by an Alfred Wegener Institute (AWI) aircraft carrying radar and laser altimeters.

3.2. Glaciological measurements

The field site at T05 experienced precipitation in the form of snow between the spring and autumn field campaigns as expected in this area of the ice sheet (Fischer et al., 1995). However, owing to surface melting, percolation into the snowpack, and subsequent refreezing, there was very little elevation change between the spring and autumn (around 5% of the annual total increase). The processes of melt and refreezing ensure that a hard surface crust is preserved at the end of each melt season. It is therefore easy in spring to dig through the winter snowpack and detect the hard relatively flat surface preserved from the previous summer. By leaving ablation stakes in place in spring 2004, it was possible to locate the same surface in autumn 2004. It was then possible to compare near surface density profiles from both spring and autumn snowpits (Fig. 3). Whilst the overall snowpack thickness is similar between spring and autumn 2004, the autumn snowpack is considerably denser, reflecting the presence of refrozen meltwater in the form of ice layers, lenses and pipes. Cores also demonstrated that the bulk of the surface densification occurred above the previous summer's melt surface.

Snow pits and cores were taken at the nine sample sites within the nested sampling grid at T05 (Fig. 1). These showed no horizontally continuous stratigraphic units within the 1 km^2. There was one exceptionally thick and spatially extensive ice layer at a depth of around 3 to 3.5 m, which was probably due to exceptional summer melting during 2002 (Ngheim et al., 2005), but even this was not present at all locations.

Very flat sastruggi ran approximately east–west covering most of the area. Surface roughness measurements were made on several scales by taking photographs of the surface against black backgrounds and digitizing the images. At T05 these showed that the surface roughness (standard deviation from a flat surface) over a measured length scale of 1.2 m was 0.91 cm in an east–west

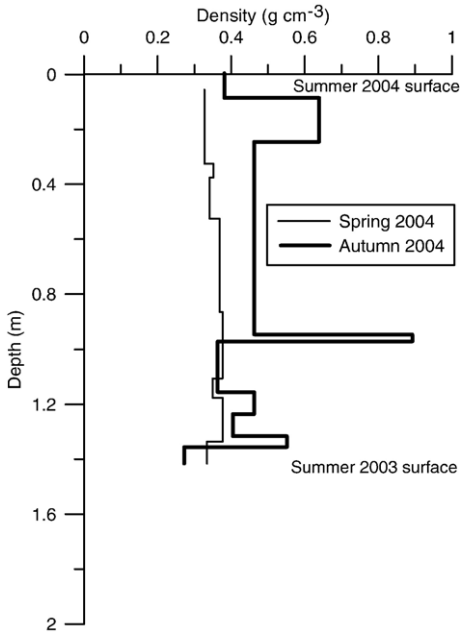

Fig. 3. Snowpit density profiles from T05E3.

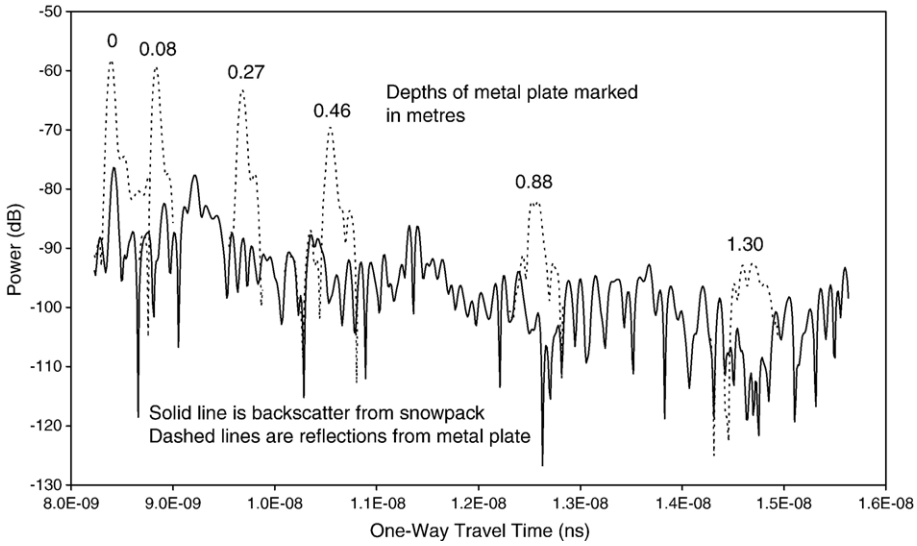

Fig. 4. Radar reflections from metal plate at T05E3. Shown alongside the general snowpack backscatter from the open snowpit with no metal plate reflector present.

direction and 1.58 cm in a north–south direction with an infinite correlation length, demonstrating the relative flatness of the surface. Micro roughness measurements over lengths of 120 mm showed that the roughness was at the measurement limit, generally on a scale of the grain size (1 mm and less) both in magnitude and wavelength. The exception to this was the area devoid of sastruggi and freshly blown snow and covered by the end summer melt surface crust. This surface crust was exposed between the sastruggi over about 25–30% of the 20 km travelled. Wavelet analysis (Torrence and Compo, 1998) demonstrated that this surface had a high magnitude roughness at length scales of around 15 mm and 35 mm. Most of the radar measurements were made over areas covered by sastruggi and freshly blown snow, the exception being those measurements over the 5 m profile (Section 5.3) which were along an area of exposed end summer surface crust.

4. Electromagnetic velocity measurements

4.1. Methodology

To calculate the velocity of the electromagnetic radiation, experiments were carried out at six snowpits (T05, T05E2, T05E3, T05E4, T05S3 and T05E1-2, located midway between T05 and T05E2) (Fig. 1). A small metal plate of dimensions $300 \times 100 \times 2$ mm was inserted into the snowpack to act as a strong radar reflector. The plate was placed at the base of the pit wall and then at decreasing depths, finishing at the surface, directly beneath the antennas. During all radar measurements the air temperature remained below −10 °C with snow temperature increasing with depth to an average of −6 °C at the base of the snow pits (around 1.5 m). This made the snow effectively 'dry', hence the real part of the dielectric constant only depended on the dielectric constants of ice and air. These are both non-dispersive and independent of temperature and frequency in the microwave region (Ulaby et al., 1986). Therefore, the main control on the electromagnetic radiation velocity should be the density of the snowpack. Since the velocity is the same at all frequencies the whole 16 GHz (2–18 GHz) bandwidth of the radar could be used for these measurements in order to locate the metal plate as accurately as possible in the snowpack.

4.2. Results

The results of the velocity calibration measurements for T05E3 are shown in Figs. 4 and 5. In Fig. 4 the reflections from the metal plate can be clearly seen above the backscatter from the snowpack. At a depth of 1.3 m the metal plate contributes proportionally much less area to the expanding wavefront and is therefore a much weaker signal. Another difficulty with the deeper measurements was the smearing of the plate reflection; this could be due to higher frequencies experiencing more random scattering (hence a spreading out of the energy) or due to multiple reflections. A larger metal plate or bar would be needed to distinguish deeper reflections over the background. The velocity remains relatively constant for this pit (Fig. 5) but was more variable in pits T05 and T05E2 owing to the presence of thicker ice lenses, which slow down the radiation. However, the positional accuracy of the reflections was inadequate to make velocity calculations for individual layers; therefore, an average velocity was calculated for each snowpit (Table 1) with greater standard deviation in this value where the velocity variations were greater. From these values the mean EM velocity for the upper metre of the snowpack was calculated to be $2.11 \pm 0.05 \times 10^8$ m s^{-1}.

For dry snow and ice the correlation between density and the real part of the dielectric constant, ε', is extremely good. Therefore, the density can be calculated from the velocity using the following equations (Glen & Paren, 1975; Ulaby et al., 1986):

$$\varepsilon' = (1 + 0.508\rho)^3 \tag{10}$$

$$v_{\text{firn}} = \frac{c}{\sqrt{\varepsilon'}} \tag{11}$$

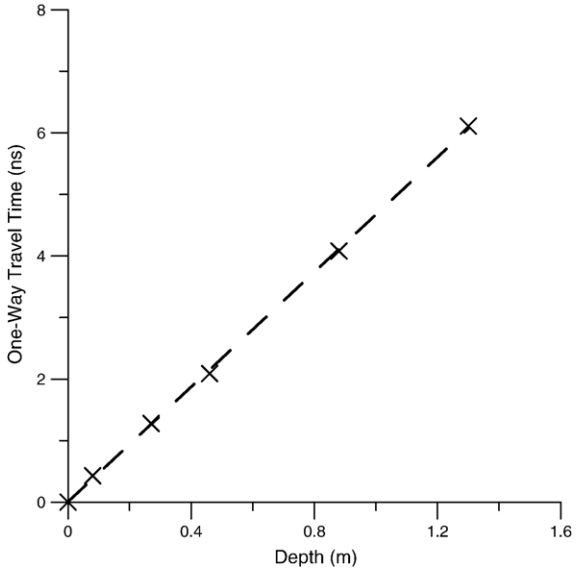

Fig. 5. Time–depth graph for metal plate velocity calculation from snowpit T05E3.

where c is the velocity of electromagnetic radiation in a vacuum, v_{firn} is the velocity in the snowpack and ρ is the density of the snowpack.

It is apparent that where there is low uncertainty in the average EM velocity, the average density derived from the radar measurements is extremely close to the average density derived from the shallow cores (Table 1). Average snowpit densities in the area show a greater difference from the radar densities. This may be because the discrete sampling of the snowpit wall is not at a high enough resolution or because hard icy layers were inadequately sampled.

5. Backscatter return and the snowpack and firn stratigraphy

5.1. General background

The snow stratigraphy in the percolation zone is extremely complex. Wind crusts, layers of depth hoar and buried sastruggi cause great variability in the permeability of the snowpack. As a result, summer melting, percolation rates, depth of meltwater penetration and subsequent refreezing are non-uniform. Ice inclusions — lenses, pipes and discontinuous layers of irregular thickness are created over the summer. Where more extreme melt events occur at lower altitudes nearer to the edge of the ice sheet, more continuous ice layers may be created. Radar measurements along a 100 m traverse by Zabel et al. (1995) at Dye-2 (66.5° N, 46.3° W) suggest that a continuous layer was present at 1 m depth with another nearly continuous layer present at 2.5 m depth. However, Dye-2 is much nearer the edge of the ice cap than T05. In 2004, a snowpit at T04 (elevation 1860 m Fig. 1) revealed greater melting, with an ice layer superimposed onto the previous summer melt horizon that was not present at T05 while a snowpit at T06 (elevation 2020 m Fig. 1) was similar in character to the pits at T05.

5.2. Results from pit and core locations

A comparison of radar measurements and firn core and snowpit density profiles at T05E3 and T05E4 is shown in Figs. 6 and 7. The firn cores, taken ~one metre from the radar measurements, demonstrate the complexity of the stratigraphy in this area. Annual layers of firn are on the order of 1 to 1.5 m thick. It is, however, not possible to identify annual horizons from depth–density fluctuations. Similar results from T05 and T05E2 demonstrate further variability in the snow stratigraphy at these locations. The firn core records include the positions of ice layers and lenses, too small to weigh separately but logged during coring, and shown as dashed lines in Figs. 6 and 7.

At a centre frequency of 13 GHz, a bandwidth higher than around 8 GHz would include measurement frequencies lower than the actual bandwidth, causing potential errors including a speckling effect from undeterminable ranges. In addition, when using frequencies lower than 9 GHz the antenna beamwidth increases significantly giving the radar system a larger area of illumination and producing significant 'sideswipe' effects. Therefore, an 8 GHz bandwidth centred on 13 GHz gave the highest resolution possible with this radar system for glaciological investigations. Using the averaged velocity of the upper metre of snowpack (see Section 4.2) gives a maximum range resolution, at 8 GHz bandwidth, of 1.3 cm by:

$$\Delta R = \frac{v_{\text{firn}}}{2 \times \text{Bandwidth}} \tag{12}$$

where ΔR is the range resolution. Radar returns calculated using a centre frequency of 13.5 GHz and a bandwidth of 1 GHz demonstrate how the resolution decreases as the lower bandwidths

Table 1
Electromagnetic radiation (EM) velocity from snowpit measurements

Snowpit	Depth to which velocity calculated with radar (m)	Average EM velocity $\times 10^8$ (m s^{-1})	Standard deviation in average EM velocity $\times$ 10^8 (m s^{-1})	Average density from EM velocity (g cm^{-3})	Standard deviation in average EM density (g cm^{-3})	Average density from core (g cm^{-3})	Average density from snowpit (g cm^{-3})
T05	0.74	2.07	0.14	0.55	0.11	0.56	0.42
T05E1-2	1.12	2.18	0.06	0.47	0.04	No result	0.52
T05E2	0.72	1.97	0.24	0.64	0.19	0.51	0.46
T05E3	1.30	2.14	0.05	0.50	0.04	0.47	0.42
T05E4	1.00	2.15	0.08	0.49	0.06	0.49	0.58
T05S3	0.55	2.12	0.01	0.51	0.01	0.49	0.54

Comparison of radar determined density with snowpit and core density. All averages are over the depth range stated in column 1.

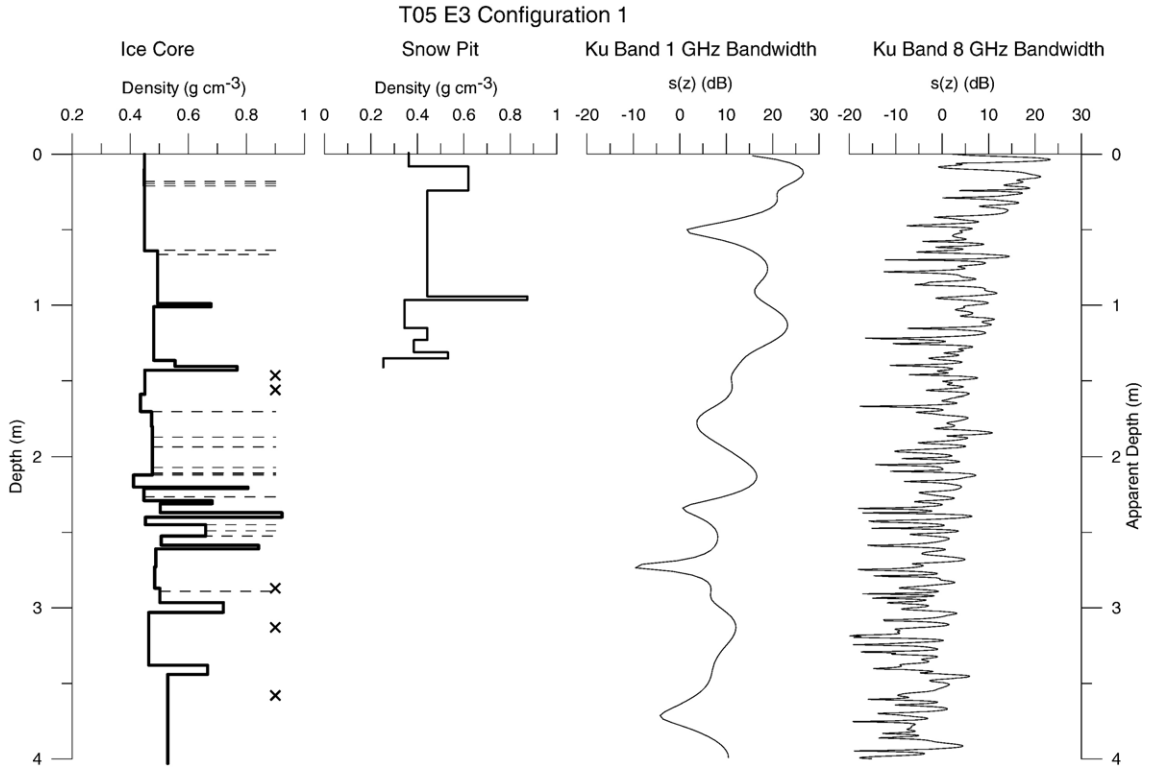

Fig. 6. T05E3. Ice core and snowpit density profiles with ice pipes (vertical dashed lines), lenses (crosses) and thin layers (horizontal dashed lines) marked on core profile. Comparison with radar measurements in the Ku band. Radar measurements are shown with a centre frequency of 13.5 GHz, bandwidth 1 GHz, and with a centre frequency of 13 GHz, bandwidth 8 GHz.

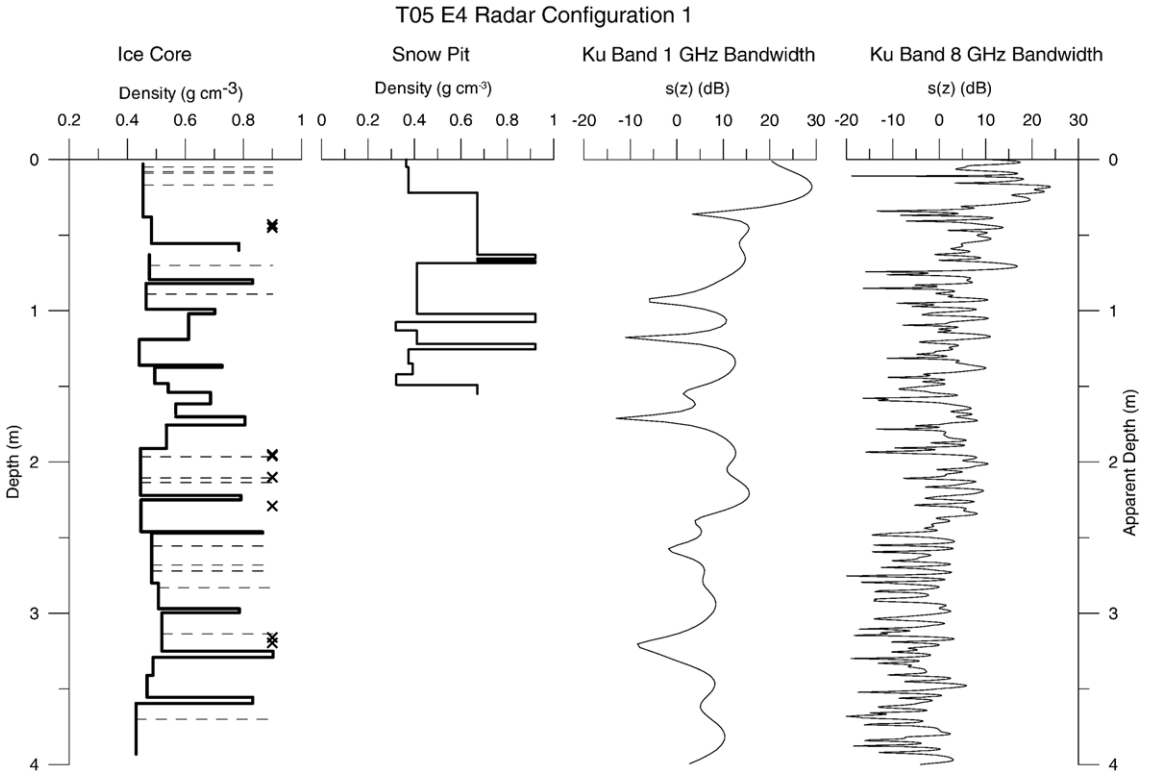

Fig. 7. T05E4. Ice core and snowpit density profiles with ice pipes (vertical dashed lines), lenses (crosses) and thin layers (horizontal dashed lines) marked on core profile. Comparison with radar measurements in the Ku band. Radar measurements are shown with a centre frequency of 13.5 GHz, bandwidth 1 GHz, and with a centre frequency of 13 GHz, bandwidth 8 GHz.

used in airborne and satellite radar altimeters are approached (Figs. 6 and 7). At this 1 GHz bandwidth the maximum range resolution would be 11 cm.

It is unsurprising that the complex stratigraphy in the percolation zone gives rise to a complex radar return with many reflectors (Figs. 6 and 7). As previously noted there is no single spatially continuous reflecting horizon across all of the radar returns from measurements at T05, T05E2, T05E3, T05E4, T05S3 and T051-2. The radar measurements have an ambiguous range of over 100 m ('wrap around' of more distant reflectors occurs only beyond this range, where they will be too weak to influence the shallow results, i.e. <10 m; Daniels, 1996) and changing the frequency step has no effect on the reflectors shown. It is therefore concluded that these are genuine primary reflections, multiples and scatterers within the snowpack. It is noteworthy that the strongest return in the 8 GHz bandwidth measurement at T05E4 originates from around 20 cm below the snowpack surface (Fig. 7). Because of the decibel scale used, this 20 cm return is significantly greater than the surface return. A strong return can also be seen from a similar depth at T05E3 (Fig. 6), but in this case the surface reflector is stronger. Measurements at the lower resolution (1 GHz bandwidth) do not resolve the ~20 cm return as separate from the surface return at T05E3/E4 (Figs. 6 and 7), but do resolve it clearly at other sites including T05 and T05E2. This is because the reflector is slightly deeper at these locations.

5.3. Results along a short 5 m profile

High resolution, 8 GHz bandwidth, measurements were also made at 0.5 m intervals along a 5 m profile (Fig. 8). The profile chosen was across a very flat end-of-summer summer melt surface to reduce complex variations in the surface reflection. This type of surface constituted around 25–30% of the total exposed surface over the 20 km travelled. Now refrozen, as air temperatures were continuously below −10 °C, it consisted of a hard, pockmarked, thin ice crust left over from the summer melting. The remaining 70–75% of the ice sheet surface in this area was covered by thin windblown snow and small sastruggi. Following radar profiling, a trench was dug to a depth of 0.5 m along the profile and the positions and thicknesses of the most continuous ice layers within the trench were recorded using a laser level (Fig. 8). These flat ice layers exhibited very low variations in amplitude on the millimetre to centimetre scale. The radar and stratigraphic surveys demonstrate that even at such short length scales there are no horizontally continuous or detectable stratigraphic horizons (Fig. 8). Instead, the results replicate the snowpit measurements whereby a series of strong reflections can be seen at several depths in the top 30 cm of the snowpack. Some of these shallower reflections would not be resolved as separate from the surface reflection at satellite bandwidths and at ~50% of the radar positions, the strongest reflector is below the surface.

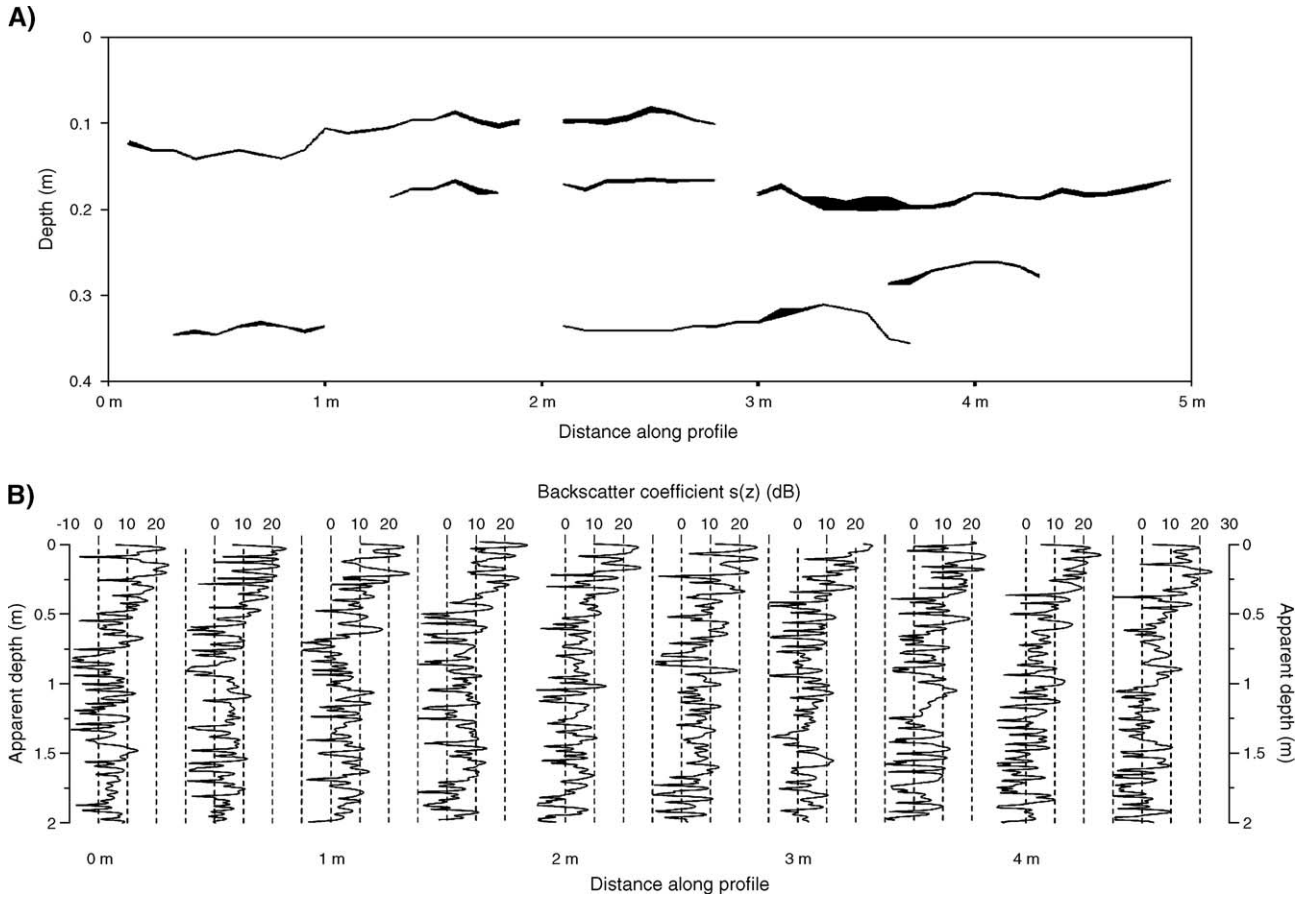

Fig. 8. Comparison along a 5 m profile of (A) continuous ice layers logged from a 0.5 m deep trench. (B) Radar measurements with 8 GHz bandwidth.

5.4. Results along a 1.5 km profile

Contouring and stacking (adding several returns together) the radar return along profiles of up to 100 m around T05 at 1 GHz and 8 GHz bandwidths gave no indication of any continuous reflecting horizons. The results above (Section 5.3) demonstrate that the return is complicated even over very short length scales. A 1.5 km radar profile was made along the EGIG line from T05 towards T06 to determine whether any reflecting horizons could be detected over longer distances. This profile consisted of 1050 radar shots. The results were smoothed horizontally using a five shot running mean and depth gain was also applied (Fig. 9) to more accurately replicate the return that would be seen by the airborne radar altimeter. Areas of shallow reflection can be seen to vary in strength along the profile with no definite continuous horizon. However, a notable horizon is present at around 1.9 to 2.0 m depth. This is not a completely continuous horizon and can disappear for sections of up to 100 m. The 1 GHz results in Figs. 6 and 7 show that a relatively strong return is present from this depth and is associated with a cluster of ice features and dense layers core. It appears that at the lower resolution and bandwidth of 1 GHz, the combination of these ice features may be responsible for this strong return. This feature is also present in the airborne radar data (data provided by ESA) and may be detectable by satellite altimeters.

6. Surface and volume backscatter results

6.1. Backscatter model

The surface and volume backscatter powers for a 1 GHz bandwidth were examined over the upper 10 m of the snowpack at seven snow-pit locations within the nested grid. The surface backscatter power can be calculated from Eqs. (4) and (6). An example of a typical distribution of backscatter power with depth in the Ku band for the upper 10 m is given in Fig. 10. The minima are cancellations due to destructive interference. A simple model, giving the variation in backscatter power with depth was used by Arthern et al. (2001) to model volume return from satellite radar. Given in terms of time, where $t=0$ is the time of the surface return, this equation is (Arthern et al., 2001):

$$s(t) = \begin{cases} \sigma^0_{\text{surf}}\delta(t) + \sigma^0_{\text{vol}} c_{\text{ice}} k_{\text{e}} \exp[-c_{\text{ice}} k_{\text{e}} t] & t \geq 0 \\ 0 & t < 0 \end{cases} \quad (13)$$

where c_{ice} is the speed of propagation within the snow; ${\sigma^0}_{\text{surf}}$ is the backscatter coefficient of the surface; δ, is the Dirac delta function; and ${\sigma^0}_{\text{vol}}$ is the integrated volume backscatter which to ensure that ${\sigma^0}_{\text{surf}} + {\sigma^0}_{\text{vol}} = \sigma^0$ is defined as (Arthern et al., 2001):

$$\sigma^0_{\text{vol}} = \frac{\sigma_{\text{v}} k_{\text{t}}^2}{2k_{\text{e}}} \quad (14)$$

where σ_{v} is the radar cross section per unit volume of snow; k_{e} is the extinction coefficient; and k_{t} is the transmission coefficient of the air–snow interface.

This model is used simply as a first step in comparing the ground results to satellite data. It may not be a physically correct model for the percolation zone but in order to upscale to the satellite footprint many ground readings would have to be averaged. Using this model, simple characteristic parameters can be extracted from the ground measurements and then used to give the strength of the surface and volume backscatter and the rate of decay with depth. There is a case for further modelling based on other models such as a coherent backscattering model.

6.2. Backscatter results

The surface backscatter parameter given in the above model was calculated separately based on the strength of the first return. The area of illumination used was the beam limited surface footprint given by Eqs. (6) and (7). The first return was then removed and the volume backscatter and extinction coefficient fitted separately to the backscatter coefficient $s(z)$ by least squares minimisation for the upper 10 m return, giving an approximate fit to the data (Fig. 10). As only the two independent parameters of gradient and magnitude were being varied it was possible to adjust them to arrive at a global minimum. This process can be used to analyse the backscatter results, by effectively reducing the backscatter to three separate parameters. The backscatter coefficients

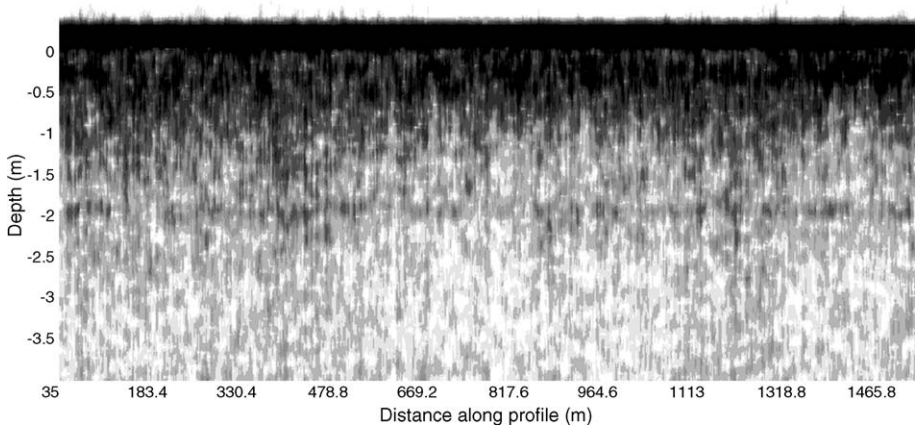

Fig. 9. 1.5 km 1 GHz bandwidth radar profile. Heading east along EGIG line from T05 (Fig. 2).

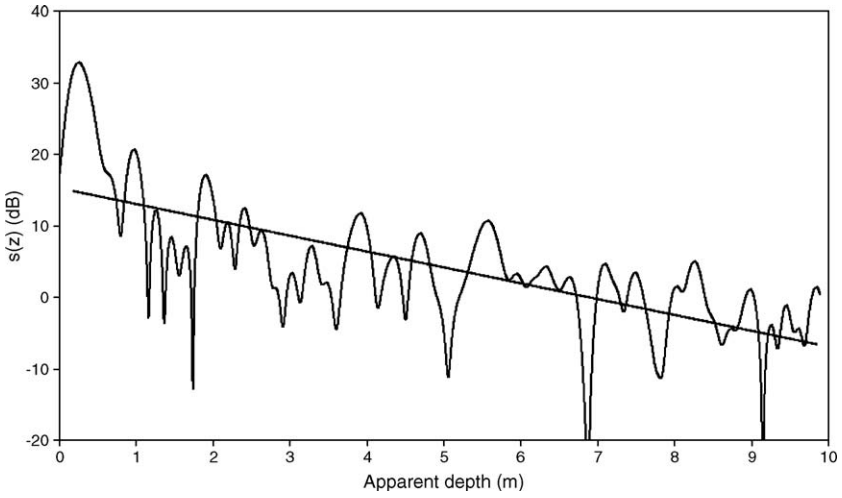

Fig. 10. T05S4 power return with best fit line.

from the model, for measurements by snowpits in the nested grid, are given in Table 2. Backscatter from all snowpits along with 14 extra measurements over the different surface covers, including sastruggi, flat summer surface and fresh windblown snow, were averaged and their ranges are given in Table 3 along with X band measurements. Backscatter parameters in the Ku band were also calculated along the trench profile from the static measurements at half metre intervals (Fig. 11, cf. Section 5.3). The backscatter coefficients were also calculated along the same profile while pulling the radar. The results corresponded closely to those from static measurements given in Fig. 11.

The backscatter values are relatively high and fall toward the upper limit of satellite altimeter backscatter values (Legresy et al., 2005). One reason for this is that the readings were made in the percolation zone after summer melt, where there are many shallow ice features, as shown above. Ulaby and Dobson (1989) give experimental results with a maximum σ^0 of 16.4 dB. This is for Ku band measurements over dry snow at vertical incidence while Kanagaratnam et al. (1997) derive values for σ^0 of 20–30 dB for Ku band backscatter over bare and pancake ice at vertical incidence, which is around the same as the backscatter values measured here.

These results (Tables 2 and 3) demonstrate that surface backscatter from structurally different snowpack surfaces is, as expected, highly variable. The profile taken over a flat end-of-summer melt surface gives a higher than average surface backscatter (Fig. 11). Surface backscatter in the X band was 2 dB lower than the Ku band but volume backscatter was the same. The extinction coefficient for Ku band is higher, that is, the return falls off more rapidly with depth at the higher frequency. This higher attenuation is expected and is probably due to loss through random scattering as the wavelength approaches the size of the snow/ice grains. For Ku measurements at nadir the surface backscatter is found to have around a 6 dB higher contribution than the volume backscatter to the total backscatter, however, this surface return includes the return beneath the surface from the upper 30 cm which is not resolved as separate at 1 GHz or less bandwidth. For X band this difference reduces to only 4 dB therefore showing volume backscatter contributes more at the lower frequency.

Table 2
Surface and volume backscatter coefficients at snowpit sites using a centre frequency of 13.5 GHz and a bandwidth of 1GHz

Snowpit location	Surface backscatter σ^0_{surf} (dB)	Volume backscatter σ^0_{vol} (dB)	Extinction coefficient k_e	Total backscatter σ^0 (dB)
T05	18	17	0.39	20
T05E1-2	28	17	0.43	29
T05E2	15	16	0.41	19
T05E3	25	18	0.42	25
T05E4	24	16	0.36	25
T05S3	20	17	0.45	22
T05S4	29	18	0.51	29

7. The return power from shallow ice layers

The results from the radar backscatter and snowpack stratigraphy (Section 5) indicate that there is often a stronger return from ice layers present in the upper 30 cm of the snowpack than from the surface. This is often not resolvable as a separate event at 1 GHz bandwidth but does have the effect of pulling the surface return down. This can be seen clearly in Fig. 7 where the peak of the surface return at 1 GHz bandwidth is close to the peak from the 8 GHz bandwidth, which appears to originate from a shallow ice layer reflection. The effect of this is to broaden the leading edge of the surface return at 1 GHz with the half power point deeper than if the reflection just originated at the surface. This finding is important as this effect would not be present before summer melting and could influence elevation estimates (and thus create errors in calculation of elevation change) from radar altimeters. It is usual to assume that the strongest backscatter to a satellite altimeter originates from the air to ice interface, with undulations in the surface and volume backscatter causing the distribution of the return. The spatial and temporal distribution of these ice layers will therefore have implications for the accuracy of calculations of annual change in ice sheet elevation.

It is useful to make a simple theoretical verification to ensure that these shallow ice layer reflectors can be stronger than the

Table 3
Average backscatter coefficients and ranges of values from static measurements at snowpit locations and areas of differing surface cover within survey area

		Surface backscatter σ^0_{surf} (dB)	Volume backscatter σ^0_{vol} (dB)	Extinction coefficient k_e	Total backscatter σ^0 (dB)
Ku band (centre frequency 13.5 GHz, bandwidth 1 GHz)	Average	24	18	0.46	25
	Standard deviation	4	1	0.06	6
	Minimum	15	16	0.36	19
	Maximum	28	20	0.59	31
X band (centre frequency 10 GHz, bandwidth 1 GHz)	Average	22	18	0.43	24
	Standard deviation	4	1	0.06	6
	Minimum	16	17	0.33	19
	Maximum	28	21	0.53	29

surface reflection. Assuming a flat surface the surface reflection coefficient, Γ, would be given by:

$$\Gamma = \frac{\sqrt{\varepsilon_{r2}} - \sqrt{\varepsilon_{r1}}}{\sqrt{\varepsilon_{r2}} + \sqrt{\varepsilon_{r1}}} \quad (15)$$

where ε_{r1} and ε_{r2} are the real relative permittivities of the two mediums. For the air to snow interface, the dielectric permittivity of air, $\varepsilon_{r1}=1$ and ε_{r2} is the dielectric permittivity of the surface snow. Taking a typical post-summer surface snow density of 0.5 g cm^{-3} gives $\Gamma=0.168$ from Eqs. (10) and (15). The reflection calculation for a thin ice layer will be different because the reflections from both the top and bottom of the layer must be taken into account. In the calculation of the internal reflections on the Greenland ice sheet, Kanagaratnam et al. (2001) also accounted for thin reflectors. In the case of a thin reflector, the equation becomes:

$$\Gamma = \frac{\sqrt{\varepsilon_{r2}} - \sqrt{\varepsilon_{r1}}}{\sqrt{\varepsilon_{r2}} + \sqrt{\varepsilon_{r1}}} 2\sin\left(\frac{2\pi l}{\lambda_2}\right) \quad (16)$$

where layer 2 is now the ice layer, l is the thickness of this layer and λ_2 is the wavelength of the electromagnetic radiation in the ice layer. To investigate whether the shallow ice layers shown in Fig. 8 can produce a higher power of reflection than the surface, Eqs. (10), (15) and (16) can be used. By assuming a typical ice layer density from core measurements of 0.86 g cm^{-3} and using the measured thicknesses of 1–16 mm for the uppermost ice layer along the profile (Fig. 8), the power reflection coefficient $|\Gamma|^2$ for both the surface and the uppermost ice layer are obtained (Fig. 12). The reflection from the ice layer is corrected by taking into account the power transmission from air to snow and back. The results demonstrate that the power return from the shallow ice layers will be highly variable along the profile because of variations in their thickness rather than their depth and in many places, the ice layers will be the strongest source of the backscatter (Fig. 12). Thus even at vertical incidence, the strongest return can vary between the surface and 30 cm depth when ice layers are present with significant implications for satellite altimeter elevation measurements, although this shallow return is unlikely to be resolvable as a separate return at satellite bandwidths. In addition, it has already been seen that the strongest return from the pre-melt spring snowpack originates from the previous summer melt surface buried under the winter accumulation (Jezek et al., 1994). This is more likely to be resolvable at satellite bandwidths but will combine with the surface return over the scale of the satellite footprint. Therefore, seasonal variability in the snowpack in the percolation zone will affect the surface return and elevation estimates.

8. The effect of millimetre scale surface roughness on the backscatter

At vertical incidence Ku band volume backscatter in the percolation zone appears to be dominated by ice layers rather than the general return from grain scattering. From laser level measurements along the trench (Section 5.3) these ice layers appear to have a roughnesses as low as that of the snow grains (<1 mm) and are therefore relatively smooth on the scale of the electromagnetic wavelength, which for 13.5 GHz is 22 mm in air and even longer in firn. Small scale surface roughness over most of the area covered by windblown snow and sastruggi is also <1 mm. The

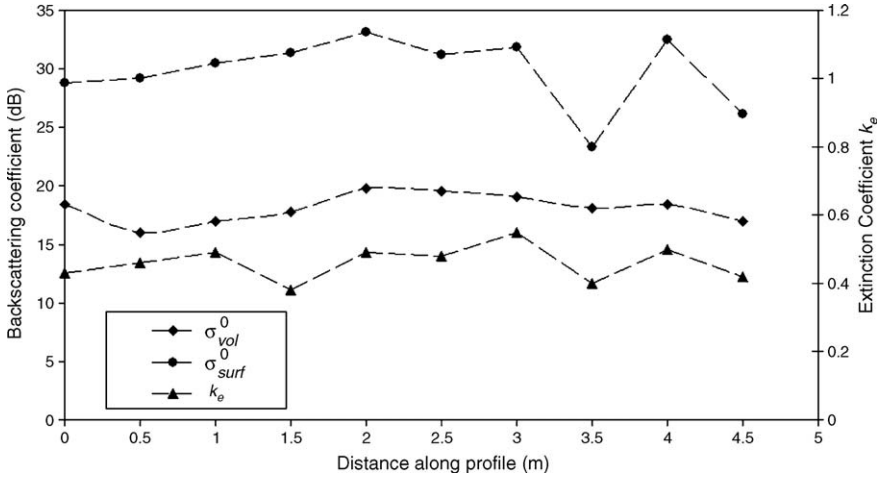

Fig. 11. Backscatter parameters along a 5 m profile. With a centre frequency of 13.5 GHz and a bandwidth of 1 GHz.

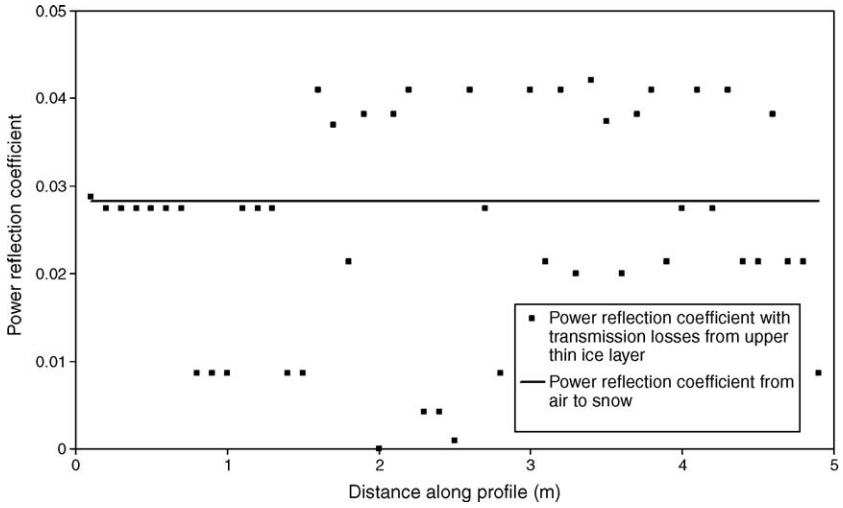

Fig. 12. Comparison of the power reflection coefficient from shallow thin ice layers (Fig. 8A) with the power reflection coefficient from the air–snow interface.

one case where small-scale roughness may be a significant factor is in the end summer melt surface. This has not been taken into account in the model above (Section 7) but with a roughness wavelength of 15 to 35 mm it would cause scattering of Ku band radiation in all directions. This may be a reason why the shallow ice layers were stronger than the surface return for 8 GHz bandwidth measurements in the area of the 5 m profile (Section 5.3) but this type of surface was not present in the measurements by snowpits (Figs. 6 and 7) and so cannot explain the relatively higher strength return of the shallow ice layers in all measurements. The higher surface backscatter values along the 5 m profile were calculated using a 1 GHz bandwidth and so these surface backscatter values are likely to include the effect of the shallow ice layers because of the lower resolution.

9. Discussion

Shallow core and snowpit observations show that the near surface snowpack/firn stratigraphy is extremely complex at the field site, ~1945 m above sea level, in the percolation zone of the Greenland Ice Sheet. There are few continuous layers within the upper 3.5 m of the firn with the horizontal extent of individual ice layers typically less than 5 m. Due to this complexity, radar returns at bandwidths of 1 GHz and 8 GHz show no traceable reflecting horizons along short profiles of less than 100 m. However, over longer profiles a discontinuous reflecting horizon, that is probably due to a collection of ice features, is present at a depth of 1.9 m. This can be seen in airborne data and so may also be detectable to satellite altimeters.

Using empirical relationships, velocity measurements from six snowpits show that mean firn densities can be derived from the radar. In the spring, prior to summer melt, it is easy to detect the depth to the previous summer melt horizon in the field. If a clear radar signal can be identified from this horizon as has been found previously, prior to summer melt (Jezek & Gogineni, 1992; Jezek et al., 1994), it could be combined with measurement of the melt horizon depth by avalanche probing. This would provide a quick and effective way of mapping the radar velocity and hence density variations in the winter snow accumulation over large areas.

Applying a basic backscatter model used by Arthern et al. (2001) simplifies the field data into the three parameters of surface backscatter, volume backscatter and extinction coefficient. These parameters are useful for examining the variation in backscatter over larger spatial and temporal scales and for quantifying the causes of variations observed in satellite data.

The discontinuity of the ice layers on such a small scale makes it difficult to combine independent sampling at several points, which should be done for continuous wave (CW) type radar systems (Ulaby et al., 1982, p. 782), and then to compare the results directly to point measurements of stratigraphy such as cores. However, the point measurements across a short profile (Section 5.3) can be used to investigate general trends in the backscatter. The backscatter parameters along the 5 m profile also closely match those calculated from mobile measurements made by pulling the radar along the profile while measuring (results not shown here). The results from all of the locations can be combined using the simple model to give an idea of the backscatter at the scale of the satellite radar footprint (Tables 1 and 3).

Our results demonstrate that the strongest return to the radar at nadir can come from thin ice layers up to 30 cm below the surface even when a hard surface crust is present (Fig. 8). It is likely that constructive interference from the top and base of these layers causes the strongest return in some locations, and that destructive interference reduces this return at other locations. At 8 GHz bandwidth this shallow ice layer return is resolved as a separate event. However, at satellite altimeter bandwidths (350 MHz for CryoSat) such a shallow reflector will not show as a separate event but instead would be merged with the actual surface return causing the surface return to broaden, making it appear deeper than if it had just been from the surface. Such shallow reflectors could be a reason for the observed discrepancies in elevation estimates derived from airborne laser and radar altimeters in this area (personal communication, Andrew Shepherd 2004). After the initial return that originates around the surface and to a depth of up to 30 cm the overall contribution of the remaining volume backscatter is found to be around 6 dB lower than the surface backscatter for Ku band, which within the context of backscatter variations across an icecap may still be significant (Legresy et al., 2005).

The results presented in this paper apply to the percolation zone, an area covering over one third of the Greenland ice sheet and which is increasing in size (Ngheim et al., 2005), but at present covers significantly less of the Antarctic ice sheet. Our findings indicate that in this zone surface measurements during both the spring and autumn are required in order to quantify seasonal differences in the backscatter properties and assess how these will effect satellite radar altimetry measurements. It is also necessary to obtain measurements from the different snowpack facies (Benson, 1962) to assess backscatter properties over larger length scales, particularly in moving between different facies (i.e. percolation into dry snow zone). As the percolation zone moves further above the 2000 m contour on Greenland (Ngheim et al., 2005) there arises a long term variation in the backscatter properties of the ice sheet, possibly adding strong backscatterers such as ice features near to the surface in areas that were formally in the dry snow zone and had a more even distribution of volume backscatter power with depth. This stronger surface and near surface return may manifest as part of the observed elevation increase in this area (Zwally et al., 2005). These measurements between facies will be part of a field campaign planned for 2006. In addition, future work will compare the field data presented above with simultaneously collected airborne radar data to assess whether our point measurements can be extrapolated to the length scales of relevance to a satellite altimeter footprint.

Acknowledgements

This paper is a contribution to the validation of the ESA CryoSat. The work was funded by the NERC through grant NER/O/S/2003/00620. The ground-based radar was constructed and tested at SPRI, Cambridge with helpful advice and guidance provided by Keith Nicholls of BAS. Our thanks for logistical support go to Kristian Keller, and Rene Forsberg of KMS, Robin Abbot of VECO Polar Resources and to Kate from KISS and to Bob Hawley for assistance in obtaining ASIRAS airborne radar data from ESA.

References

Arthern, R. J., Wingham, D. J., & Ridout, A. L. (2001). Controls on ERS altimeter measurements over ice sheets: Footprint-scale topography, backscatter fluctuations, and the dependence of microwave penetration depth on satellite orientation. *Journal of Geophysical Research*, *106*(D24), 33471−33484.

Benson, C. S. (1962). Stratigraphic studies in the snow and firn of the Greenland ice sheet. SIPRE Research Report 70.

Bindschadler, R. (1998). Monitoring ice sheet behaviour from space. *Reviews of Geophysics*, *36*, 79−104.

Corr, H. F. J., Jenkins, A., Nicholls, K. W., & Doake, C. S. M. (2002). Precise measurement of changes in ice-shelf thickness by phase-sensitive radar to determine basal melt rates. *Geophysical Research Letters*, *29*(8), doi:10.1029/2001GL014618

Daniels, D. J. (1996). Surface penetrating radar. *IEE Radar, Sonar, Navigation and Avionics Series*, *6*.

Drinkwater, M. R., Long, D. G., & Bingham, A. W. (2001). Greenland snow accumulation estimates from satellite radar data. *Journal of Geophysical Research*, *106*(D24), 33935−33950.

Drinkwater, M. R., Francis, R., Ratier, G., & Wingham, D. J. (2003). The European Space Agency's Earth explorer mission CryoSat: Measuring variability in the cryosphere. *Annals of Glaciology*, *39*, 39A236.

Fischer, H., Wagenbach, D., Laternser, M., & Haeberi, W. (1995). Glaciological and isotopic studies along the EGIG line, central Greenland. *Journal of Glaciology*, *41*, 515−527.

Glen, J. W., & Paren, P. G. (1975). The electrical properties of snow and ice. *Journal of Glaciology*, *15*, 15−38.

Jezek, K., & Gogineni, S. (1992). Microwave remote sensing on the Greenland ice sheet. *IEEE Geoscience and Remote Sensing Society Newsletter*, *9*, 6−10.

Jezek, K. C., Gogineni, P., & Shanableh, M. (1994). Radar measurements of melt zones on the Greenland ice sheet. *Geophysical Research Letters*, *21*, 33−36.

Kanagaratnam, P., Gogineni, S. P., Gundestrup, N., & Larsen, L. (2001). High-resolution radar mapping of internal layers at the North Greenland Ice Core Project. *Journal of Geophysical Research*, *106*(D24), 33799−33811.

Kanagaratnam, P., Gogineni, S., Jezek, K., Peters, L., Young, J., & Zabel, I. (1997). Ultra-wideband radar measurements over bare, snow-covered and pancake ice. *RSL Technical Report* (pp. 12100−12101).

Legresy, B., Papa, F., Remy, F., Vinay, G., van den Bosch, M., & Zanife, O. -Z. (2005). ENVISAT radar altimeter measurements over continental surfaces and ice caps using the ICE-2 retracking algorithm. *Remote Sensing of Environment*, *95*, 150−163.

Legresy, B., & Remy, F. (1997). Altimetric observations of surface characteristics of the Antarctic ice sheet. *Journal of Glaciology*, *43*, 265−275.

Ngheim, S. V., Steffen, K., Neumann, G., & Huff, R. (2005). Mapping of ice layer extent and snow accumulation in the percolation zone of the Greenland ice sheet. *Journal of Geophysical Research*, *110*(F2), F02017.

Torrence, C., & Compo, G. P. (1998). A practical guide to wavelet analysis. *Bulletin of the American Meteorological Society*, *79*, 61−78.

Ulaby, F. T., & Dobson, M. C. (1989). *Handbook of Radar Scattering: Statistics for Terrain.* Dedham, Massachusetts: Artech House.

Ulaby, F. T., Moore, R. K., & Fung, A. K. (1982). *Microwave remote sensing: Active and passive*, *vol. II*. Reading, Massachusetts: Addison-Wesley.

Ulaby, F. T., Moore, R. K., & Fung, A. K. (1986). *Microwave remote sensing: Active and passive*, *vol. III*. Reading, Massachusetts: Addison-Wesley.

Wingham, D. J. (1995). A method of determining the average height of a large topographic ice sheet from observations of the echo received by a satellite altimeter. *Journal of Glaciology*, *41*, 125−141.

Zabel, I. H. H., Jezek, K. C., Baggeroer, P. A., & Gogineni, S. P. (1995). Ground-based radar observations of snow stratigraphy and melt processes in the percolation facies of the Greenland ice sheet. *Annals of Glaciology*, *21*, 40−44.

Zwally, H. J., Giovinetto, M. B., Li, J., Cornejo, H. G., Beckley, M. A., Brenner, A., et al. (2005). Mass changes of the Greenland and Antarctic ice sheets and shelves and contributions to sea-level rise: 1992–2002. *Journal of Glaciology*, *51*, 509−527.